

3-D Relativistic MHD Simulations

K.-I. Nishikawa¹, J. Frank², S. Koide³, J.-i. Sakai³,
D. M. Christodoulou², H. Sol⁴, and R. L. Mutel⁵

(1) *Department of Physics and Astronomy,
Rutgers, The State University of New Jersey,*

136 Frelinghuysen Road Piscataway, NJ 08854-8019 USA

(2) *Department of Physics and Astronomy, Louisiana State University,
Baton Rouge, LA 70803-4001, USA*

(3) *Laboratory of Plasma Physics and Fusion Science, Faculty of Engineering,
Toyama University, Gofuku, Toyama 930, Japan*

(4) *DARC, Observatoire de Paris-Meudon, 5, place Jules Janssen,
92195 Meudon Cedex, France*

(5) *Department of Physics & Astronomy, University of Iowa
Iowa City, IA 52242, USA*

E-mail: kenichi@physics.rutgers.edu, frank@rouge.phys.lsu.edu,

koidesin@ecs.toyama-u.ac.jp, sakaijun@ecs.toyama-u.ac.jp,

Helene.Sol@obspm.fr, rlm@astro.physics.uiowa.edu

Abstract. We present 3-D numerical simulations of moderately hot, supersonic jets propagating initially along or obliquely to the field lines of a denser magnetized background medium with Lorentz factors of $W = 4.56$ and evolving in a four-dimensional spacetime. (a) Parallel-injection case—Compared to previous simulations in two spatial dimensions, the resulting structure and kinematics differ noticeably: the density of the Mach disk is lower and the head speed is smaller. This is because the impacted ambient fluid and its embedded magnetic field make efficient use of the third spatial dimension as they are deflected circularly off of the head of the jet. As a result, a significant magnetic-field component normal to the jet is created near the head. If the field is strong, backflow and field reversals are strongly suppressed; upstream, the field closes back on the surface of the beam and assists the collimation of the jet. If the field is weak, backflow and field reversals are more pronounced, although still not as extended as in the corresponding plane-parallel case. In all models, the high-pressure region is localized near the jet head irrespective of the presence/strength of the magnetic field; and the head decelerates efficiently by transferring momentum to the background fluid which recedes along a thin bow shock in all directions. (b) Oblique-injection case—Our simulations show that relatively weak, oblique fields (at 1/16 of the equipartition value) have only a negligible influence on the propagating jet and they are passively pushed away by the relativistically moving head; in contrast, oblique fields in equipartition with the ambient plasma provide more resistance and cause bending at the jet head, but the magnitude of this deflection and the associated backflow are small compared to those identified by previous studies. The new results are understood as follows: Relativistic simulations have consistently shown that these jets are effectively heavy and so they do not suffer substantial momentum losses and are not decelerated as efficiently as their nonrelativistic counterparts. In addition, the ambient magnetic field, however strong, can be pushed aside with relative ease by the beam, provided that the degrees of freedom associated with all three spatial dimensions are followed self-consistently in the simulations. This effect is analogous to pushing Japanese “noren” or vertical Venetian blinds out of the way while the slats are allowed to bend in 3-D space rather than as a 2-D slab structure.

1. Introduction

VLBI observations of superluminal ejections from the centers of quasars and BL Lacertae objects (e.g., Gabuzda, Wardle, & Roberts 1989, [1]; Mutel et al. 1990, [2]; Cawthorne 1991, [3]; Gabuzda et al. 1992, [4]; Fejes, Porcas, & Akujor 1992, [5]; Hummel et al. 1992, [6], 1992, [7]; Ghisellini et al. 1993, [8]; Conway & Davis 1994, [9]; Biretta, Zhou, & Owen 1995, [10]; Wardle & Aaron 1996, [11]) and VLA/VLBI observations of Galactic X-ray sources (e.g., Mirabel & Rodríguez 1994, [12]; Hjellming & Rupen 1995, [13]) have established that jet outflows commonly occur with speeds near the speed of light and that the outflowing material in extragalactic sources does not slow down to nonrelativistic speeds out to kiloparsec scales. The surrounding intergalactic and interstellar media in which these jets propagate are clearly magnetized and often show, even on very large scales, a well-organized magnetic-field structure. Ordered magnetic fields of several microgauss have been observed on kiloparsec scales in the centers of some clusters of galaxies such as Coma and Hydra A (Kim et al. 1990, [14]; Crusius-Watzel et al. 1990, [15]; Taylor & Perley 1993, [16]). Even stronger magnetic fields are expected on smaller scales, in the close surroundings of active galactic nuclei, because of compression and amplification of any frozen-in magnetic fields (e.g., Soker & Sarazin 1990, [17]) carried by accretion flows that are infalling toward the “central engine.” Regarding the stellar case, many jets emanating from young stellar objects (YSOs) are aligned with the local interstellar magnetic field (Reipurth 1989, [18]). Non-aligned stellar jets are also observed but they could be related to the presence of a binary star system at the central source (Reipurth 1997, [19]). These results suggest that the interstellar magnetic field plays, at some level, a primary role to the dynamics of YSO jets, although binarity at the source could mask the magnetic influence (e.g., by changing the angular momentum vector of the accreted matter).

In the case of extragalactic jets, there are many unresolved problems concerning curvature effects and the observed distortions. One long-standing question is the peculiar morphology of wide-angle-tail radio galaxies which does not admit any direct explanation in terms of external or ram pressures, gravitational effects, motion of the host galaxy, collisions with intergalactic clouds, or electric current-carrying jets (Eilek et al. 1984, [20]; O’Donoghue, Owen, & Eilek 1990, [21], 1993, [22]). Another puzzling enigma is the secondary peak found at about 90° in the distribution of misalignment angles between VLBI (parsec) jets and their extensions on kiloparsec scales (Pearson & Readhead 1988, [23]; Wehrle et al. 1992, [24]; Conway & Murphy 1993, [25]; Xu et al. 1994, [26]; Appl, Sol, & Vicente 1996, [27]). Other specific features observed in samples of distorted radio jets—such as the sharp bends observed in the three superluminal quasars 3C 216, 3C 309.1, and 3C 345—are also difficult to model without introducing too many free parameters in the fits.

In this paper, we discuss the parallel propagation of relativistic jets. We also pursue the idea that relativistic jets can be deflected by an external magnetic field. The elemental process of this bending mechanism, which is the deflection of a relativistically propagating beam by a strong magnetic field embedded in the surrounding medium, has been previously studied in three spatial dimensions (3-D) in the nonrelativistic domain (Koide et al. 1996, [28], hereafter, KSNM) and in a two-dimensional (2-D) slab geometry using a relativistic magnetohydrodynamics (RMHD) computer code (Koide 1997, [29]). The computer code that we are currently using is an outgrowth of this 2-D RMHD code but the algorithm follows the time-

evolution of plasma and magnetic field in all three spatial dimensions (see Koide, Nishikawa, & Mutel 1996, [30], hereafter, KNM) for details and tests of the numerical scheme). Allowing for both 3-D relativistic and 3-D magnetic effects is also what distinguishes this code from other codes that have been used by various researchers to study relativistic jets in 2-D with or without magnetic fields (e.g., van Putten 1993, [31], 1996, [32]; Duncan & Hughes 1994, [33]; Martí, Müller, & Ibáñez 1994, [34]; Martí et al. 1995, [35], 1996, [36], 1997, [37]; Koide, Nishikawa, & Mutel 1996, [30]; Komissarov & Falle 1996, [38], 1997, [39]; Koide 1997, [29]).

We discuss results obtained from fully 3-D RMHD jet simulations carried out for a brief period of time and at a modest grid resolution of 101^3 zones. In § 2, we discuss the influence of both 3-D and relativistic effects for the parallel and oblique injections. A summary of our discussions is presented in § 3.

2. Initial Conditions and Numerical Results

The relevant initial conditions have also been described by Nishikawa et al. (1997) [40] who studied relativistic jets injected along magnetic-field lines (“parallel-injection” case). For the present “oblique-injection” simulations, we also employ a Cartesian XYZ grid with 101 equally-spaced zones in each direction (Nishikawa et al. 1998, [41], 1998 [42]). The computational box is a cube that occupies the region $0 \leq X \leq 20$, $-10 \leq Y, Z \leq 10$. This box is filled uniformly with fluid of rest mass density $\rho_a = 1$, pressure $P_a = 0.6$, and specific energy $\epsilon_a = 0.9$; a uniform magnetic field B is also embedded at an initial angle of 0° (parallel case) and 45° (oblique case) to the XY -plane. At times $t \geq 0$, jet material of rest mass density $\rho_j = 0.3$ ($\eta \equiv \rho_j/\rho_a = 0.3$) and specific energy $\epsilon_j = 3$ is injected in the X -direction from an orifice at $X = 0$, $Y^2 + Z^2 \leq 1$. The jet’s proper pressure is initially equal to the thermal pressure of the ambient medium. No symmetry is assumed across any of the boundaries during evolution. In addition, fixed-inflow and radiative boundary conditions are implemented at the $X = 0$ surface and at all the other surfaces, respectively. Thus, the propagation of the jet can be followed only for a relatively brief period of time spanning ≤ 20 initial jet radii.

We express velocities in units of the sound speed $v_s = (\gamma P_a / (\rho_a + \gamma P_a / (\gamma - 1)))^{1/2}$ in the ambient medium (where $v_s = (\gamma P_a / \rho_a)^{1/2} \equiv 1$) and we measure time in units of τ_s , the transit time of a sound wave over unit distance. In addition, we choose an adiabatic index of $\gamma = 5/3$ for the fluid and an injection speed v_j that leads to a proper Mach number of $M_j \equiv v_j/v_s = 4$ and a Lorentz factor of $W_j = (1 - v_j^2/c^2)^{-1/2} = 4.56$ ($v_j/c = 0.9756$ for $c = 4.1v_s$).

Each simulation requires more than 1 Gbyte of dynamic memory and takes about 35 CPU hours on the Power Challenge of the National Center for Supercomputing Applications. We have so far carried out two comparative runs characterized by different strengths of the initial magnetic field ($B_{X0} = B_0 \cos \theta$ and $B_{Z0} = B_0 \sin \theta$ with $\theta = 0^\circ$ (parallel; Runs A and B), and 45° (oblique; Runs C and D)): in Runs A and C, the energy density of the field, $B_0^2/2$, was equal to $5/9$ of the internal energy density, $\rho_a \epsilon_a$, of the ambient plasma (i.e., $B_0 = 1$ and Alfvén speed $v_A \equiv B_0 \rho_a^{-1/2} = v_s$); in Runs B and D, the energy density of the field was reduced by a factor of 16 (i.e., $B_0 = 0.25$ and $v_A = 0.25v_s$). In addition, the condition $B_{Z0} = 0$ was implemented at $X = 0$ to avoid numerical problems at the orifice.

- Parallel Case

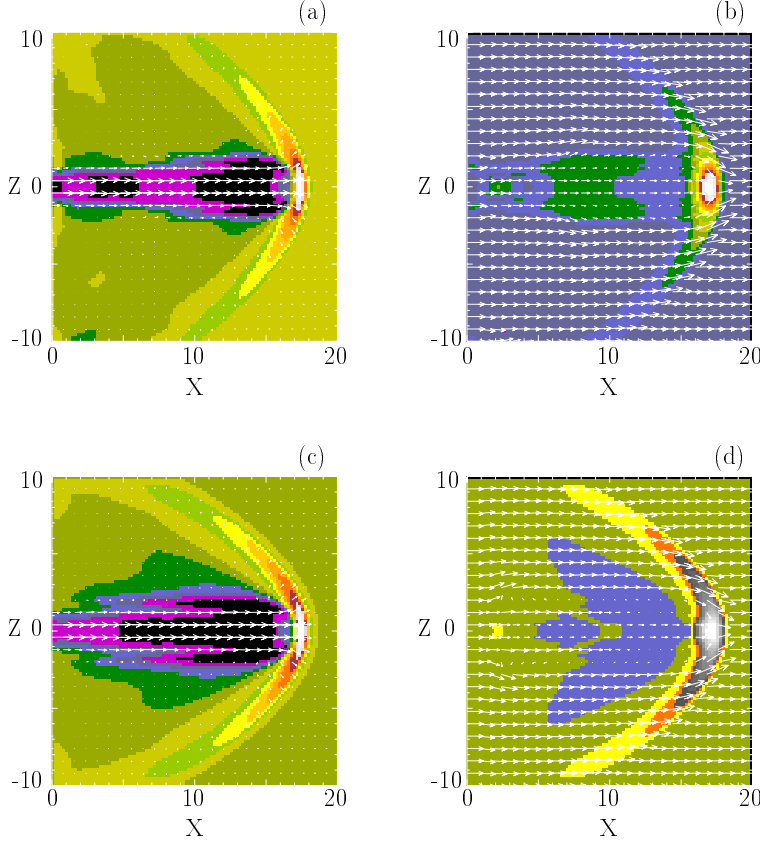


Figure 1. Run A (panels a,b) and Run B (panels c,d) with strong and weak magnetic field, respectively: XZ cross-sections through $Y = 0$ at $t = 8.5\tau_s$. Panels a,c show contours of rest mass density and velocity vectors. Panels b,d show contours of thermal pressure and magnetic-field vectors. The maximum values represented by white color are: (a) $\rho_{\max} = 1.94$; (b) $P_{\max} = 3.29$; (c) $\rho_{\max} = 2.17$; and (d) $P_{\max} = 3.64$.

Figures 1a,b and Figures 1c,d show various MHD variables on the $Y = 0$ plane at $t = 8.5\tau_s$ for Runs A and B, respectively. Figures 1a,c depict the rest mass density and the velocity, while Figs. 1b,d depict the thermal pressure and the magnetic field. (Horizontal $[XY]$ cross-sections at $Z = 0$ reveal very much the same morphology, while YZ cross-sections show the overall axisymmetry of the jets.) In both cases, the Mach disks (Figs. 1a,c) are almost at the same location, $X \approx 17$, because the average propagation speeds of the relativistic jet heads are almost the same: $v_h = 2.06v_s$. (In more detail, the heads slow down to the following average speeds: $v_h = 2.17v_s$ for $0 < t < 3.0\tau_s$, $2.10v_s$ for $3.0\tau_s < t < 6.0\tau_s$, and $1.88v_s$ for $6.0\tau_s < t < 8.5\tau_s$.) Although higher than the one-dimensional (1-D) nonrelativistic estimate of $v_h = \eta^{1/2}(1 + \eta^{1/2})^{-1}v_j = 1.42v_s$, this average speed is significantly smaller than both the 2-D value of $v_h = 2.67v_s$ found by KNM and the corresponding 1-D relativistic nonmagnetic estimate (e.g., Martí et al. 1996, [36]) of $v_h = \eta_R^{1/2}(1 + \eta_R^{1/2})^{-1}v_j = 2.92v_s$, where the relativistic inertia ratio $\eta_R \equiv \eta(h_j/h_a)W_j^2 = 7.42$ and $h \equiv 1 + (\epsilon + P/\rho)/c^2$

denotes the relativistic specific enthalpy. The observed head speed is in-between the above relativistic and nonrelativistic estimates. This outcome is clearly due to a combination of relativistic and three-dimensional effects: Lorentz contraction increases the effective mass density of the jet and hence its thrust and average speed, but the head of the beam is decelerated by the ambient medium more strongly in 3-D than in 2-D; hence, an average propagation efficiency of only $2.06/2.92 = 70\%$ is achieved because of more efficient momentum transfer to the impacted 3-D fluid.

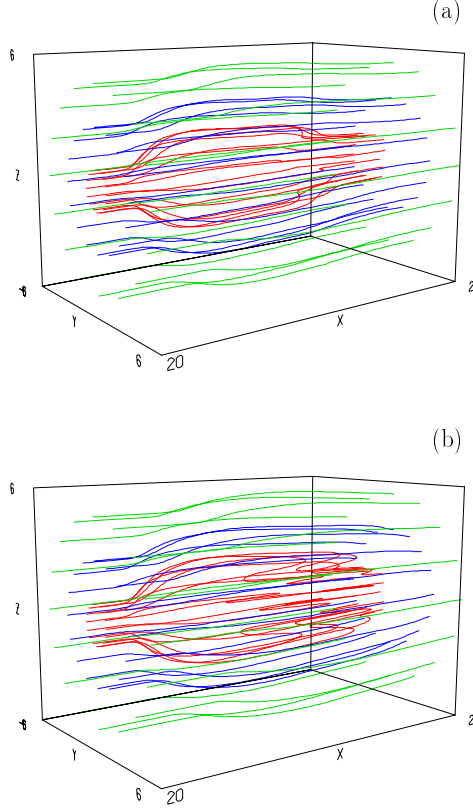


Figure 2. (a) Run A and (b) Run B: field lines in 3-D space at $t = 8.5\tau_s$ from a viewpoint in front and to the side of the jet. Red, blue, and green lines are traced starting at the front side ($X = 19.8$) from a radius of $(Y^2 + Z^2)^{1/2} = 1, 3$, and 5 , respectively.

Comparing the two cases, the transverse propagation of the bow shock is faster in Run A (Figs. 1a,b) because the fast magnetosonic waves are faster in the strongly magnetized medium. Also, the width of the bow shock in Run A is smaller because the shocked ambient flow is not affected substantially by backflow as the magnetic field is deflected by the head less than in Run B (see Fig. 2 below). In relation to the 2-D case, however, the widths of both 3-D bow shocks are smaller and their tips are

closer to the beams (see Figs. 1 and 2 in KNM).

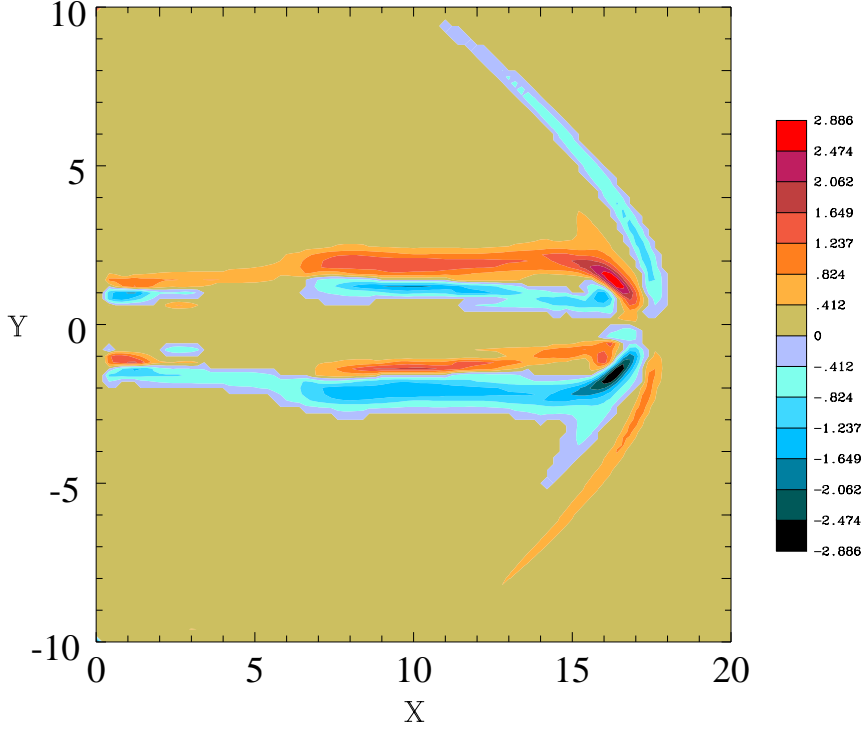


Figure 3. Horizontal (XY) cross-section through $Z = 0$ at $t = 8.5\tau_s$ for the strongly magnetized run showing the distribution of three different electric currents (J_Z). Currents shown in red/blue color recede/approach the observer. Two currents circle near the surface of the cylindrical beam and a third current circles around the bow shock.

The density of the Mach disk and the head pressure are both higher by $\sim 10\%$ in the weak-field Run B. In both runs, however, the high-pressure region is strongly localized around the head (Figs. 1b,d). This feature is also due to 3-D effects because it is not observed in the 2-D simulations of KNM. The localization occurs because there is no preferred direction for momentum transfer in the 3-D runs, leading to more efficient matter transport away from the head.

Figure 1c shows “wings” of pronounced backflow forming beside the jet in Run B. With the exception of a thin surface layer behind the head, no such feature develops in the strong-field case. The absence of backflow in Fig. 1a is similar to the result obtained by Martí et al. (1996) [36] from a nonmagnetic 2-D simulation of a considerably hotter jet. It seems then that either a strong, aligned magnetic field in the ambient medium or a high internal specific energy in the jet can independently prevent backflow and cocoon turbulence.

One of the best ways to illustrate structural details on the head and the surface of the jet is to trace the magnetic-field lines in 3-D space. This is shown in Fig. 2 for Runs A (Fig. 2a) and B (Fig. 2b) at $t = 8.5\tau_s$. The observer is located in front and to the side of the approaching beam. The following features are readily apparent: (1) bending of the field lines (rotational discontinuity) at the location of the bow shock; (2) a flared region behind the head inside of which the ambient field has been canceled by a current induced around the beam; and (3) confining, straight field lines upstream along the surface of the beam in Run A and pronounced field-line reversals in Run B (*red curves*).

In Run A (Fig. 2a), the strong magnetic field that is pushed away by the propagating beam is deflected almost circularly; as a result, it develops significant normal components (on the YZ plane), comparable to the X -components. The field closes back on the beam upstream and contributes to the confinement of the exceptionally thin and internally featureless jet (Figs. 1a, 2a). Although deflected in a similar fashion, the field in Run B (Fig. 2b) is too weak to play the same role. Thus, the weak magnetic field in Run B does not influence the propagation and collimation of the jet which evolves very much as in the nonmagnetic Run N and results in the formation of a significantly less confined beam (Figs. 1c, 2b). This is consistent with the fact that the field lines (red) in Fig. 2a are less expanded outside than those in Fig. 2b. In addition, Fig. 2b shows that the reversal of field lines in Run B is limited near the surface of the beam. By comparison, Fig. 2a shows only a hint of very small field reversals in Run A. In the corresponding 2-D cases (KNM), both field-line reversals and backflowing wings are more pronounced and more extended.

The regions where the magnetic field is near zero (Figs. 1b,d) indicate the location of the induced current whose density distribution $\mathbf{J} \equiv \nabla \times \mathbf{B}$ is quite complex as shown in Fig. 3 for Run A: Two distinct, concentric, roughly cylindrical surfaces with toroidal current form near the surface of the beam and approach each other near the head; and another current circulates on the bow shock. The currents on the bow shock and the inner cylindrical surface have the same polarity which is opposite to that of the current on the outer cylindrical surface. All three currents are generated from the interaction of the jet with the ambient plasma in places where the magnetic-field lines are bent or canceled as described above.

We finally note that a deviation of the beam from its original path has been observed during these simulations and longer time-integrations are needed in order to find out whether this effect is the beginning of nonlinear head oscillations analogous to those seen in nonmagnetic nonrelativistic 3-D jets (Norman 1993, [43]). At the end-point of our runs, the heads of the jets are displaced by a few grid cells relative to the original direction of propagation. A displacement of this magnitude is not sufficient to produce pronounced asymmetries in the leading section of the beam. Its presence is however revealed on the bow shock in Fig. 3, where the circulating current appears to be off-centered.

- Oblique Case

Figures 4a,b and Figures 4c,d show various MHD variables on the XZ -plane at $t = 8.0\tau_s$ for Runs C and D, respectively. Figures 4a,c depict the rest mass density and the velocity, while Figs. 4b,d depict the thermal pressure and the magnetic field. The Mach disks are located at $X \approx 14.5$ (Run C) and $X \approx 16.0$ (Run D) because the average propagation speed of the head in Run C ($v_h = 1.81v_s$) is reduced by the resisting magnetic field. The corresponding value in Run D, $v_h = 2.00v_s$, is effectively

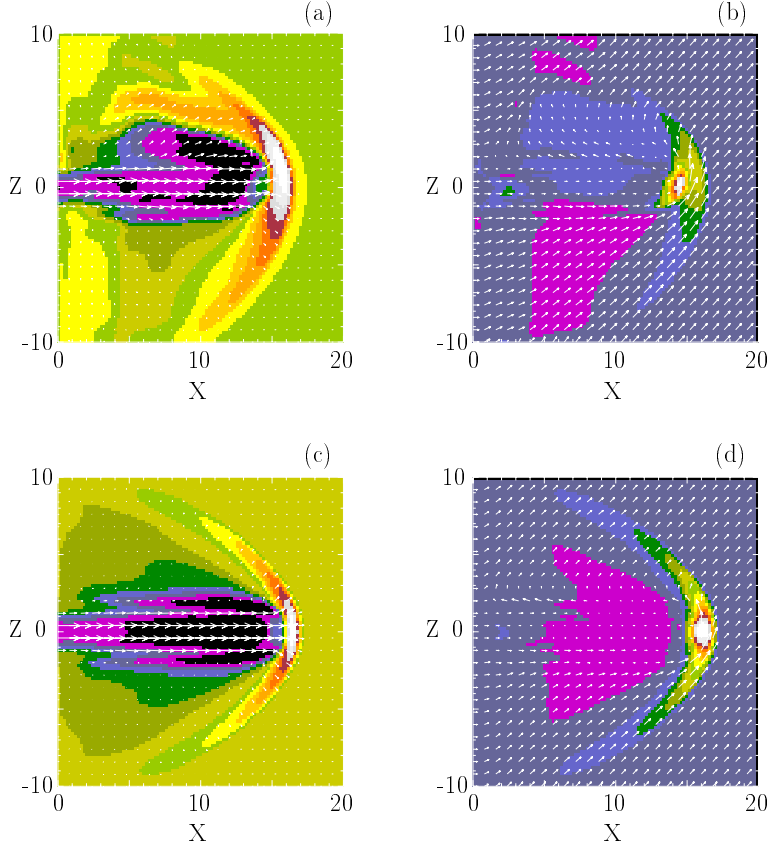


Figure 4. Run C (panels a,b) and Run D (panels c,d) with strong and weak magnetic field, respectively: XZ (vertical) cross-sections through $Y = 0$ at $t = 8.0\tau_s$. Panels a,c show contours of rest mass density and velocity vectors. Panels b,d show contours of thermal pressure and magnetic-field vectors. The maximum values represented by white color are: (a) $\rho_{\max} = 1.68$; (b) $P_{\max} = 3.56$; (c) $\rho_{\max} = 2.17$; and (d) $P_{\max} = 3.70$.

the same as that obtained by Nishikawa et al. (1997, [40]) in the parallel-injection runs. This indicates that the weak oblique field in Run D has a negligible influence on the kinematics of the jet. In Run C, we have also measured the average head speed at $t = 7.0\tau_s$ for comparison with the corresponding 2-D run of Koide (1997) [29]. We have found that $v_h = 1.85v_s$, a value considerably larger than $v_h = 1.57v_s$ obtained in 2-D. This comparison implies that the jet can propagate faster and easier in 3-D by pushing the field lines out of the way and by slipping through the opening just as people do when they get through a Japanese “noren” or push vertical Venetian blinds to the side.

In the strongly magnetized Run C, the jet is deflected above the $Z = 0$ plane, but the bending is not as strong as in the corresponding 2-D RMHD run. As a result

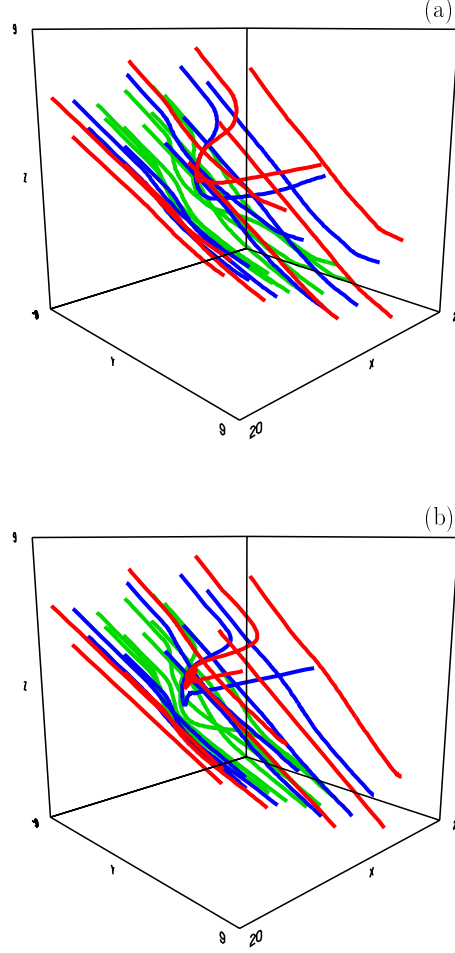


Figure 5. (a) Run C and (b) Run D: field lines in 3-D space at $t = 8.0\tau_s$ from a viewpoint in front and to the side of the jet. Green (8), blue (8), and red (8) lines are traced starting at the front side ($14.0 \leq X \leq 19.8$ $X = -1.933 * Z + 29.46$ for $Z \geq 5.0$ and $X = 19.8$ for $Z < 5.0$) from the points $((Y/2.0)^2 + (Z - 5.0)^2)^{1/2} = 1$ (green), 2 (blue), and 3 (red), respectively.

of bending and compression at the head, the high-pressure region is offset from the high-density region (Fig. 4a,b). This feature is not seen in the weakly magnetized Run D (Fig. 4c,d) which proceeds just as the corresponding parallel-injection run (Run B in Nishikawa et al. 1997, [40]). Furthermore, because the jet slips through the magnetic field, strong backflow and large-scale vortical motions do not develop in these runs. The shock “wings” seen in Run D are consistent with those seen in the parallel-injection case. In Run C, the limited flow away from the surface of the beam is asymmetric. A weak reverse flow develops on the lower section of the beam (Fig. 4a) where the field has been pushed down by the jet and the field lines are now parallel to the direction of propagation (Fig. 4b). The plasma is forced to follow field lines. Above

the jet, the outflow is more substantial and more extended, which is illustrated as a bending process by Soker (1997) [44]. This material then develops a “forward” flow (at about $30^\circ - 45^\circ$ to the XY -plane) and inflates the asymmetric cocoon seen in Fig. 4a between the upper surface of the beam and the strongly distorted part of the bow shock. Finally, comparing Run C to Run D, we see that the transverse propagation of the bow shock is faster in Run C, owing to the increased fast magnetosonic speed in the strongly magnetized ambient medium; and the width of the bow shock in Run C is much larger because the stronger field resists more and creates a larger pile-up of field lines.

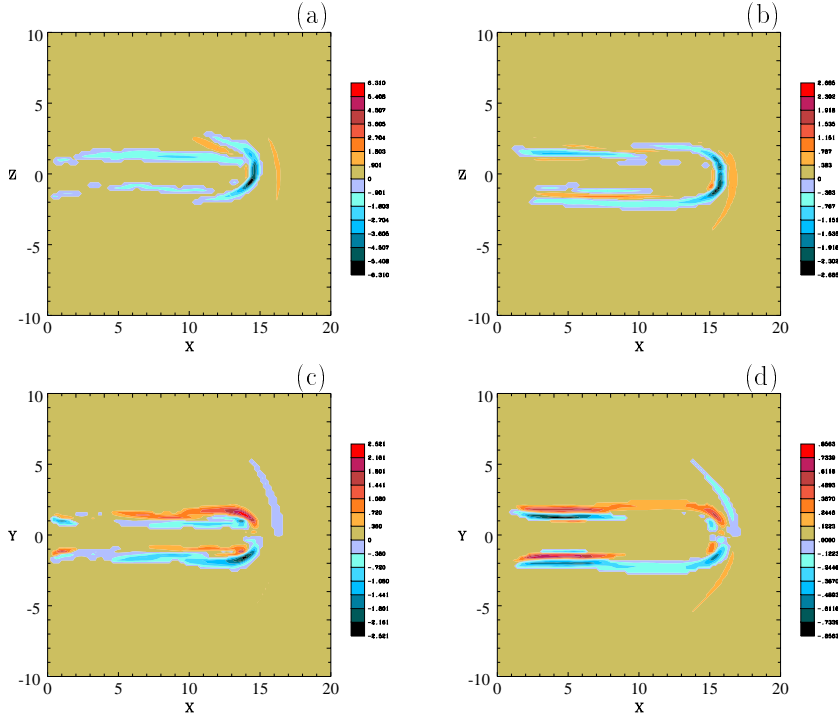


Figure 6. Contours of the electric currents for Run C (panels a,c) and Run D (panels b,d) at $t = 8.0\tau_8$: (a,b) the J_Y component on the XZ -plane; (c,d) the J_Z component on the XY -plane. In all panels the currents are normal to the corresponding planes and are colored in red or blue color according to whether they recede or approach the observer.

For comparison with the corresponding 3-D nonrelativistic case with $\theta = 45^\circ$, we refer to the results from Cases D ($M_j = 4$) and E ($M_j = 7$) of KSNM. The most striking features of those runs were strong reversals of the field lines above the deflected jet and field cancellation on the surface of the beam by the generated current. Fig. 4 shows that, although bent, the magnetic field in the RMHD runs does not at all suffer

large-scale reversals above the jet. On the other hand, the field is canceled near the surface of the relativistic beam where localized reversals do occur on the interface between the jet plasma and the ambient medium, but this effect was also observed in the parallel-injection case; thus, localized field reversals cannot be used to characterize jets produced by oblique injection. Instead, special attention should be given to the electric currents that develop on the surfaces of the beams because their characteristics do change in the oblique-injection case as will be discussed later.

One of the best ways to illustrate the interaction between the jet and the oblique magnetic field is to trace the magnetic-field lines in 3-D space. This is shown in Fig. 5 for Runs C (Fig. 5a) and D (Fig. 5b) at $t = 8.0\tau_s$. The observer is located in front and to the side of the approaching beam. The unperturbed magnetic field lines lie approximately on concentric elliptical cylinders with the innermost (8) lines in green, the outermost (8) lines in red, and the (8) blue lines in between. The green lines are such that they threaded through the jethead near its head.

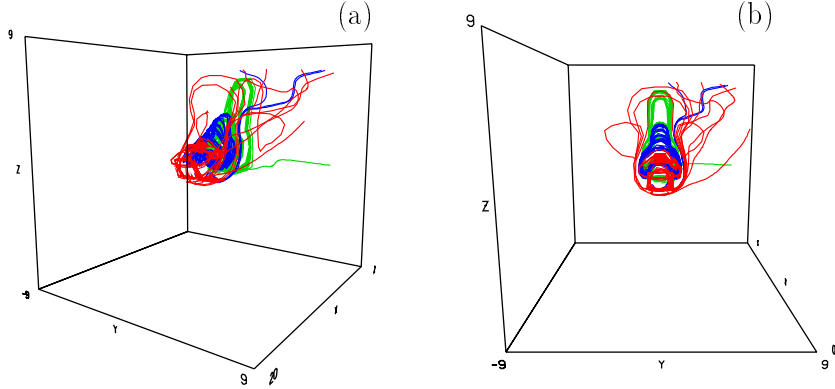


Figure 7. Flow lines of electric current for Run C in 3-D space at $t = 8.0\tau_s$ (a) from a viewpoint in front and to the side of the jet and (b) from a viewpoint in front of the jet. Red (8), blue (8), and green (8) lines are traced starting at the back side ($X = 14, 12, 10$) around circles with radii $(Y^2 + Z^2)^{1/2} = 1.0$, respectively.

As shown in Fig. 5a,b, in the plane at the center of the jet ($Y = 0$) the three most bent field lines which start from $(X, Z) = (14.0, 8.0)$ (red), $(15.9, 7.0)$ (blue), $(17.9, 6.0)$ (green) are strongly disturbed by the jet. These magnetic field lines are bent in a similar way as shown in Fig. 2 by Soker (1997) [44] (see also the arrows in Fig. 4b,d). These three field lines are piled up near the jethead where the magnetic field is intensified. The red and blue field lines are connected with the magnetic field in the jet. On the other hand, the green magnetic field lines are just bent without being connected with the jet.

It should be noted that shapes of these three field lines are different due to the different strength of the ambient magnetic field. For example, the red field line shown in Fig. 5a is bent far from the jet due to the stronger piled-up magnetic field than in

Fig. 5b). In weak-field case (Fig. 5b), the red and blue lines are not only dragged along by the jet, but also bent back near the jethead in a kind of “hook.” The field reversals are clearly recognized with these dragged field lines. Faraday rotation measurement can be attributed to the interaction of the jet with the oblique magnetic fields as suggested by Soker (1997) [44].

As a summary, the following features are readily apparent:

- (1) bending of the field lines due to the pressure at the location of the jethead;
- (2) the field lines which are dragged in both cases connect to the magnetic field lines near the center of the jets; and
- (3) field lines (green) near the jet are bent aside in both sides (Y -direction) of the jet.

The distribution of electric current density $\mathbf{J} \equiv \nabla \times \mathbf{B}$ on the XZ (vertical) and XY (horizontal) planes is illustrated in Fig. 6. This complex distribution is generated from the interaction of the jet with the oblique magnetic field. As in the parallel-injection runs, currents generally flow on the bow shock and on the surface of the beam. The present runs reveal, however, several important differences which can be used to identify and recognize jet propagation into an oblique magnetic field:

- (a) The current on the bow shock is weak, not very extended spatially, and strongly asymmetric. This is because the field is mostly bent above and near the head of the jet.
- (b) As shown in Fig. 6a,b, the strong currents behind the bow shock at $X \approx 15$ (dark blue) correspond to field lines that have been piled up and carried by the central regions of the jets. The enhanced magnetic field is recognized in the Mach disk as shown in Fig. 4b,d. These currents are localized at $Y = 0$ and their distances from the weak currents on the front sides of the bow shocks (orange) are consistent with the thicknesses of the bow shocks seen in Fig. 4.
- (c) In the upper section of the beam on the XZ -plane, field lines have been reversed and canceled as shown in Fig. 4b,d. The resulting current loops are no longer circular and situated on YZ -planes.

In order to show the noncircular current around the jet, Figure 7 shows the flow lines of electric currents for Run C in 3-D simulation space. In order to show the 3-D structure effectively, two view angles are chosen (a) from the front and side of the jet and (b) from the straight ahead of the jet. The flow lines are traced from the three different jet locations ($X = 14$ (red), 12 (blue), 10 (green)) at the edge of the jet. For example, red flow lines start at equally-spaced eight points at $X = 14$, and $Y^2 + Z^2 = 1$ near the jethead ($X = 15$). As shown in Fig. 7, the current flow lines are tilted backwards and are elongated in the $+Z$ -direction. In addition, the loops are not round on the lower side of the jet and the currents form a configuration that looks like a half saddle (in particular with blue curves above the jet) rather than a collection of parallel circular loops.

(d) In the lower section of the beam on the XZ -plane, field lines have also been dragged by the jet in a way that produces a second component of electric current that flows roughly on the surface of the beam (*red and blue lines* on the lower parts of Fig. 7). Consequently, all these asymmetries imposed on the magnetic field prevent the formation of well-organized, concentric, cylindrical currents such as those found in the parallel-injection case.

Comparing the currents in Runs C and D (i.e., Figs. 6a,c to Figs. 6b,d), we see that their distributions are qualitatively similar. As expected, the currents in Run D are weaker by factors of 2 – 3, owing to the lower strength of the magnetic field. In addition, the XY and XZ cross-sectional areas of each beam are obviously unequal,

indicating that the jet is no longer circular. In particular for Run C, the beams are wider on the XY -plane where they have to actively push the field lines to the side. On the XZ -plane where the field provides bending, the lower part of the surface layers of the beam are pushed upward and the jet remains slender.

3. Discussions

We have performed 3-D RMHD jet simulations in which the relativistic beam encounters an ambient magnetic field (parallel and oblique). Both parallel-injection case (Nishikawa et al. 1997, [40]) and oblique-injection case (Nishikawa et al. 1998, [41], 1998, [42]) show how important the inclusion of 3-D effects is to the resulting morphology and propagation characteristics.

In the parallel case, in contrast to the 2-D case, we have found that moderately hot 3-D relativistic beams decelerate more efficiently, develop no internal structures, and maintain circular currents at parts of their surfaces and small localized heads of lower density and pressure; and that the associated bow shocks are considerably thinner and stay closer to the beams. Furthermore, the jets are better collimated and show no strong backflows or significant field reversals in the presence of dynamically important ambient magnetic fields. A strong magnetic field is temporarily pushed away by the head almost axisymmetrically, but returns to confine the beam farther upstream. In the cases of weak or no magnetic field, backflowing wings and pronounced field reversals do develop, but they are not as strong as in the corresponding 2-D plane-parallel cases studied by KNM; hence, the lesser but significant confinement of the jet is entirely due to relativistic effects.

On the contrary, as was expected from previous nonrelativistic 3-D simulations (KSNM), the resisting field lines are deflected away by the head of the jet instead of being dragged downstream; the ambient medium and its magnetic field that are compressed at the tip of the head have only a small influence on the propagation of the jet. As a result, the beam can easily slip through the magnetic field (unlike in the 2-D slab case). Furthermore, because the jet is relativistic, the plasma does not suffer substantial momentum losses as observed in the 3-D nonrelativistic computations. Neither the 3-D relativistic effects nor the 3-D magnetic effects favor the development of irregular large-scale kinematics. Thus, if the ambient medium is weakly magnetized the jet propagates just as in the parallel-injection case. If the embedded field is in equipartition with the ambient plasma, then:

- (a) the beam suffers a deflection, but the bending is not as strong as in the previously studied cases and the jet slows down very little—note, however, that bending may increase over longer timescales;
- (b) flow away from the beam occurs mostly in the upper section, where the plasma follows the oblique field lines and moves forward (i.e., in the direction of deflection) without generating reverse vortices or backflowing wings on large scales;
- (c) the head speed is significantly larger than that in the 2-D slab case although its value is $\sim 10\%$ lower than that obtained in the parallel-injection case;
- (d) electric currents flow predominantly on the surface of the beam, where they create complicated asymmetric patterns which include both partial circulation around the beam and partial flow along the direction of propagation of the jet.

We will continue to do more simulations with different parameters and with a longer system. We will also compare simulation results with observations.

4. Future Research

- Jet Variabilities

We also propose to add perturbations in the initial conditions for injected jets such as density, velocity, and internal energy, which are supposed to be caused in the process of jet generation (e.g. Tsvetanov et al 1998, [45]). Three possible explanations for the observed variability are (i) tidal disruption of a star falling into the black hole (Hills 1997, [46]), (ii) instabilities in the relativistic accretion disk (Sunyaev 1973, [47]; Shakura & Sunyaev 1973, [48]), and (iii) jet-related processes (Kollgaard 1994, [49]; Camenzind & Krockenberger 1992, [50]). Based on these theories and observations (e.g. Reid 1998, [51]), for example, the initial density is perturbed with a small fraction 1 - 10 % (including an intermitted jet) ($n_{inj} = n_0 + \delta n(t)$). Another possible additional perturbation is the initial jet velocity. Several ways are considered: 1) δv_x along the jet axis, 2) $\delta v_{y,z} (= \delta v_\theta)$ caused by the precession, and 3) combination of both. These initial conditions will be properly chosen based on the observations of M87 and 3C345 and the simulation results with uniform jets. We expect helical instability to occur at the jet boundary layer and we will investigate the possible observed consequences of these effects.

- Helical Magnetic Field inside jets

In the processes of generating jets, the magnetic fields inside the jet are twisted (e.g. Koide et al. 1998, [52]). The helical magnetic field inside jets may produce knots in jets (van Putten 1996, [32]). Simulations with a helical magnetic field in a jet have been performed. This investigation is in progress.

- Jet Generation Simulations using a 3-D GRMHD code

Koide et al (1998, [52], 1999, [53]) have investigated the dynamics of an accretion disk initially threaded by a uniform poloidal magnetic field in a non-rotating corona (either in a steady-state falling state or in hydrostatic equilibrium) around a non-rotating black hole using a 3-D GRMHD with the axisymmetry. The numerical results show the followings: As time goes on, the disk loses angular momentum by magnetic braking, and falls onto a black hole. The infalling motion of the disk, which is faster than in the non-relativistic case because of general relativistic effect below $3 r_S$ (r_S is the Schwarzschild radius), is strongly decelerated around $r = 2r_S$ by the centrifugal force to form a shock inside the disk. Magnetic field is tightly twisted by the rotation of the disk, and plasmas in the shocked region of the disk are accelerated by $\mathbf{J} \times \mathbf{B}$ force to form bipolar relativistic jets.

In order to investigate variabilities of generated relativistic jets and magnetic field structure inside jets, we have performed the 3-D GRMHD code with a full 3-dimensional system. This investigation is in progress.

Acknowledgments

This work was supported in part by the U.S-Japan cooperative science program JSPS and by NSF (INT-9217650); by NSF grants ATM-9119814, ATM-9121116, ATM-9730230; and by supercomputing grants at NCSA and PSC.

References

- [1] Gabuzda, D. C., Wardle, J. F. C., & Roberts, D. H. 1989, *ApJ*, 336, L59
- [2] Mutel, R. L., Phillips, R. B., Su, B., & Bucciferro, R. R. 1990, *ApJ*, 352, 81
- [3] Cawthorne, T. V. 1991, in *Beams and Jets in Astrophysics*, ed. P. A. Hughes (Cambridge: Cambridge Univ. Press), 187
- [4] Gabuzda, D. C., Cawthorne, T. V., Roberts, D. H., & Wardle, J. F. C. 1992, *ApJ*, 388, 40
- [5] Fejes, R., Porcas, R. W., & Akujor, C. E. 1992, *A&A*, 257, 459
- [6] Hummel, C. A., Muxlow, T. W. B., Krichbaum, T. P., Quirrenbach, A., et al. 1992, *A&A*, 266, 93
- [7] Hummel, C. A., Schalinski, C. J., Krichbaum, T. P., Rioja, M.J., et al. 1992, *A&A*, 257, 489
- [8] Ghisellini, G., Padovani, P., Celotti, A., & Maraschi, L. 1993, *ApJ*, 407, 65
- [9] Conway, J. E., & Davis, R. 1994, *A&A*, 284, 724
- [10] Biretta, J. A., Zhou, F., & Owen, F. N. 1995, *ApJ*, 447, 582
- [11] Wardle, J. F. C., & Aaron, S. E. 1996, in *Energy Transport in Radio Galaxies and Quasars*, ASP Conf. Ser., 100, 123
- [12] Mirabel, I. F., & Rodríguez, L. F. 1994, *Nature*, 371, 46
- [13] Hjellming, R. M., & Rupen, M. P. 1995, *Nature*, 375, 464
- [14] Kim, K.-T., Kronberg, P. P., Dewdney, P. E., & Landecker, T. L. 1990, *ApJ*, 355, 29
- [15] Crusius-Watzel, A., Biermann, P. L., Lerche, I., & Schlickeiser, R. 1990, *ApJ*, 360, 417
- [16] Taylor, G. B., & Perley, R. A. 1993, *ApJ*, 416, 554
- [17] Soker, N., & Sarazin, C. L. 1990, *ApJ*, 348, 73
- [18] Reipurth, B. 1989, *AA*, 220, 249, also in *1st Results from Observations of Southern Star Forming Regions with the Swedish ESO Submillimeter Telescope*, ed. M. Olberg, B. Reipurth, & R. S. Booth (Garching bei München: ESO), 247
- [19] Reipurth, B. 1997, private communication
- [20] Eilek, J. A., Burns, J. O., O'Dea, C. P., & Owen, F. N. 1984, *ApJ*, 278, 37
- [21] O'Donoghue, A. A., Owen, F. N., & Eilek, J. A. 1990, *ApJ*, 72, 75
- [22] O'Donoghue, A. A., Owen, F. N., Eilek, J. A. 1993, *ApJ*, 408, 428
- [23] Pearson, T. J., Readhead, A. C. S. 1988, *ApJ*, 328, 114
- [24] Wehrle, A. E., Cohen, M. H., Unwin, S. C., Aller, H. D., Aller, M. F., & Nicolson, G. 1992, *ApJ*, 391, 589
- [25] Conway, J. E., & Murphy, D. W. 1993, *ApJ*, 411, 89
- [26] Xu, W., Readhead, A. C. S., Pearson, T. J., Wilkinson, P. N., & Polatidis, A. G. 1994, in *Compact Extragalactic Radio Sources*, ed. J. A. Zensus & K. I. Kellerman (Green Bank: NRAO), 7
- [27] Appl, S., Sol, H., & Vicente, L. 1996, *A&A*, 310, 419
- [28] Koide, S., Sakai, J., Nishikawa, K.-I., & Mutel, R. L. 1996, *ApJ*, 464, 724 (KSNM)
- [29] Koide, S. 1997, *ApJ*, 478, L66
- [30] Koide, S., Nishikawa, K.-I., & Mutel, R. L. 1996, *ApJ*, 463, L71 (KNM)
- [31] van Putten, M. H. P. M. 1993, *ApJ*, 408, L21
- [32] van Putten, M. H. P. M. 1996, *ApJ*, 467, L57
- [33] Duncan, G. C., & Hughes, P. A. 1994, *ApJ*, 436, L119
- [34] Martí, J. M^a, Müller, E., & Ibáñez, J. M^a. 1994, *A&A*, 281, L9
- [35] Martí, J. M^a, Müller, E., Font, J. A., & Ibáñez, J. M^a. 1995, *ApJ*, 448, L105
- [36] Martí, J. M^a, Font, J. A., Ibáñez, J. M^a, & Müller, E. 1996, in *Energy Transport in Radio Galaxies and Quasars*, ASP Conf. Ser., 100, 149
- [37] Martí, J. M^a, Font, J. A., Ibáñez, J. M^a, Müller, E., & Marquina, A. 1997, *ApJ*, 478, 151
- [38] Komissarov, S. S., & Falle, S. A. E. G. 1996, in *Energy Transport in Radio Galaxies and Quasars*, ASP Conf. Ser., 100, 173
- [39] Komissarov, S. S., & Falle, S. A. E. G. 1997, *MNRAS*, 288, 833
- [40] Nishikawa, K.-I., Koide, S., Sakai, J., Christodoulou, D. M., Sol, H., & Mutel, R. L. 1997, *ApJ*, 483, L45
- [41] Nishikawa, K.-I., Koide, S., Sakai, J., Christodoulou, D. M., Sol, H., & Mutel, R. L. 1998, *ApJ*, 498, 166.
- [42] Nishikawa, K.-I., J. Frank, D. M. Christodoulou, Koide, S., Sakai, J., Sol, H., & Mutel, R. L. 1998, *New Astron. Rev.*, 42, 633.
- [43] Norman, M. L. 1993, in *Astrophysical Jets*, edited by D. Burgarella, M. Livio & C. O'Dea, p. 211.
- [44] Soker, N. 1997, *ApJ*, 488, 572
- [45] Tsvetanov, Z. I., Hartig, G. F., Ford, H. C., Dopita, M. A., Kriss, G. A., Pei, Y. C. Dressel, L.

- L., & Harms, R. J., 1998, ApJ, 493, L83.
- [46] Hills, J. G., 1997, Nature, 254, 295.
 - [47] Sunyaev, R. A., 1973, Soviet Astron., 16, 941.
 - [48] Shakura, N. I., & Sunyaev, R. A., 1973, A&A, 24, 337.
 - [49] Kollgaard, R. I., Vista Astron., 38, 29.
 - [50] Camenzind, M. & Krockenberger, M., 1992, A&A, 255, 59.
 - [51] Reid, M., 1998, Science, 281, 1815.
 - [52] Koide, S., Shibata, K. and Kudoh, T., 1998, ApJ, 495, L63.
 - [53] Koide, S., Shibata, K. and Kudoh, T., 1999, ApJ, accepted.